*Sensors & Transducers, Vol. 226, Issue 10, October 2018, pp. 71-76*

www.sensorsportal.com

**Sensors & Transducers**

Published by IFSA Publishing, S. L., 2018
http://www.sensorsportal.com

# Simulation of Light Scattering by a Pendent Drop with Statistic Vectorial Complex Ray Model

**Ruiping YANG, Claude ROZÉ, Saïd IDLAHCEN and * Kuan Fang REN**
UMR 6614/CORIA, Normandie Université, CNRS-Université et INSA de Rouen, Site du Madrillet, Avenue de l'Université, BP 12, 76801 Saint-Etienne du Rouvray, France
Tel.: +33 232953743, fax: +33 232910485
* E-mail: fang.ren@coria.fr

*Received: 25 June 2018 /Accepted: 31 August 2018 /Published: 31 October 2018*

**Abstract:** Due to the new property of wave front curvature in the Vectorial Complex Ray Model (VCRM), the later permits to simulate with good precision the scattering of large non-spherical particles. This communication presents an exploration of the model with a statistic algorithm – Statistic Vectorial Complex Ray Model (SVCRM), in which the light wave is presented by photons having the same properties of rays in VCRM and the total scattered intensity is calculated statistically by summation of intensity of all photons arriving in the same box in given direction. An analytical description of scattered intensity without interference on a non-spherical object by a plane wave is investigated. And the orders of rays are considered and their corresponding intensity distributions are numerically simulated. Simulated results of scattered field are presented and compared with scattering patterns obtained experimentally for a pendant water droplet. The skeletons of the numerical and experimental patterns are in good agreement. The scattering mechanism of different order rays is revealed.

**Keywords:** light scattering, non-spherical particles, Statistic Vectorial Complex Ray Model, geometrical optics, optical metrology, pendent drop.

## 1. Introduction

Optical metrology is wildly used in many applications, such as multiphase flows, combustion, etc. to retrieve properties of the system under study. To reach this end, we need to establish the relation between the properties of the scattered light and those of the scatterers. Various theories and models have been developed to deal with the scattering of light by particles but none of them can predict with precision the scattering of large non-spherical particles. Rigorous theories [1], such as Lorenz-Mie theory, are applicable only to particles of simple shapes [2]. Numerical methods, such as T-Matrix, the discrete dipole approximation (DDA) and the finite-difference time-domain (FDTD), can predict the scattering of particles of complex shapes, but the size of the particles is very limited. Approximate models, such as geometrical optics (GO), can deal with the scattering of large particles of any shape, but its precision is often not sufficient. Furthermore, it is very difficult to take into account the divergence / convergence of a wave on the surface of the particle.

The scattering of large non-spherical particle is therefore a bottleneck problem in the optical metrology. In order to overcome this obstacle, we have developed Vectorial Complex Ray Model (VCRM) [3-4] for the scattering of light / electro-magnetic waves by large particles of smooth surface and arbitrary shape, which has been validated numerically [5] and experimentally [6] in the cases of scattering in a symmetric plane of scatterer.

In order to extend the applications of the model in more common scattering problems, we must develop algorithms for three dimension objects. VCRM permits to calculate the complex amplitude of each ray but to obtain the total scattering we need to count contribution of all rays arriving at the same angle. To this end, a statistic version of VCRM, called here after statistic VCRM (SVCRM), has been proposed, in which the total scattered intensity is calculated statistically by summation of the intensity of all rays/photons arriving in boxes in given direction [7].

## 2. Research Models

### 2.1. Vectorial Complex Ray Model

In VCRM, all waves are described by bundles of vectorial complex rays and each ray is characterized by its propagation direction, polarization, phase, amplitude as well as a new property – *wave front curvature*. Thanks to this new property, the divergence of the wave on the particle surface and the phase due to the focal line are counted very easily. And the evolution of the wave front curvature at each interaction is described by the wave front equation [3-4]:

$$(\mathbf{k}'-\mathbf{k})\cdot\mathbf{n}\cdot\mathbf{C}=k'\Theta'^{T}\mathbf{Q}\Theta'-k\Theta^{T}\mathbf{Q}\Theta\,, \qquad (1)$$

where $\mathbf{n}$ is for the normal of dioptric surface, $\mathbf{k}$ and $\mathbf{k}'$ are the wave vectors of the rays before and after interaction, $k$ and $k'$ the corresponding wave numbers. $\mathbf{C}$ is the curvature matrix of the dioptric surface at the incident point. $\mathbf{Q}$ and $\mathbf{Q}'$ are respectively the wave front curvature matrix of the waves before and after interaction. $\Theta$ and $\Theta'$ are the projection matrix of the bases of $\mathbf{C}$ with that of $\mathbf{Q}$ and $\mathbf{Q}'$ respectively.

Furthermore, to simplify the calculation, only the wave vector components are used in VCRM to determine the direction and the Fresnel coefficients. The Snell law in vector form is just the continuous of the tangent component of wave vectors before and after interaction $k_\tau$ and $k_\tau^{'}$ namely:

$$k_\tau = k_\tau^{'} \qquad (2)$$

### 2.2. Statistic Vectorial Complex Ray Model

In SVCRM, we describe all five properties of ray mentioned above in four normalized orthogonal bases: $(\mathbf{x}_\mathbf{i}^{(s)},\mathbf{x}_\mathbf{j}^{(s)},\mathbf{n})$ for the particle surface, $(\mathbf{x}_\mathbf{i}^{(i)},\mathbf{x}_\mathbf{j}^{(i)},\mathbf{x}_\mathbf{k}^{(i)})$ $(\mathbf{x}_\mathbf{i}^{(r)},\mathbf{x}_\mathbf{j}^{(r)},\mathbf{x}_\mathbf{k}^{(r)})$ and $(\mathbf{x}_\mathbf{i}^{(t)},\mathbf{x}_\mathbf{j}^{(t)},\mathbf{x}_\mathbf{k}^{(t)})$ for the incident rays, the reflected rays and the refracted rays respectively.

#### 2.2.1. Location of Interaction Point

At a given interaction point of a ray with the particle surface, the four normalized orthogonal bases are illustrated in Fig. 1. The incidence plane is defined by the propagation direction of the incident wave and the normal to the surface $\mathbf{n}$, which is oriented from the side of the incident ray to the side of the refraction ray. $\theta_i$ is the incident angle and $\theta_t$ is the refraction angle.

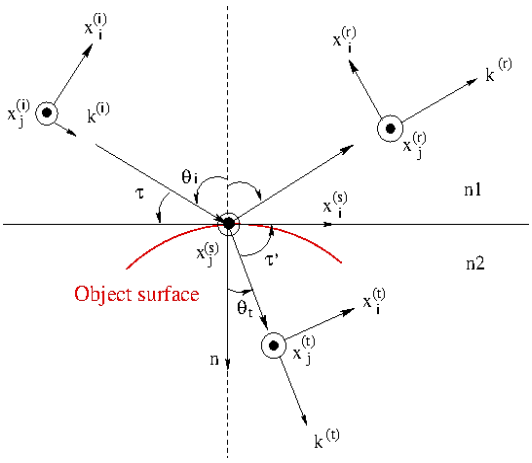



**Fig. 1.** Four normalized orthogonal bases at the interaction point on the surface of a non-spherical object and the definition of their directions.

According to the Snell laws in vector form, the directions of the reflection ray and the refraction ray are related to the direction of the incident ray $\mathbf{x}_\mathbf{k}^{(i)}$ by:

$$\begin{aligned}\mathbf{x}_\mathbf{k}^{(r)} &= \mathbf{x}_\mathbf{k}^{(i)} - 2\cos\theta_i\mathbf{n}\\ \mathbf{x}_\mathbf{k}^{(t)} &= \frac{1}{\rho}\mathbf{x}_\mathbf{k}^{(i)} + (\cos\theta_t - \frac{1}{\rho}\cos\theta_i)\mathbf{n}\end{aligned}, \qquad (3)$$

where $\rho = n_2/n_1$.

For a given ray defined by a starting point $\boldsymbol{r}(x_0,y_0,z_0)$ and a propagation direction $\mathbf{u}$, and a dioptric surface described by three dimensions function $\boldsymbol{r}=\boldsymbol{r}(x,y,z)$, the next interaction point is then the solution of the following equation

$$\boldsymbol{r}(x_0,y_0,z_0)+\alpha\boldsymbol{u}=\boldsymbol{r}(x,y,z)\,, \qquad (4)$$

where $\alpha$ is the propagation distance.

In our simulation, the polar coordinates are used to describe the droplet profile. For that, a center is defined at $(y_c=0, z_c=750)$. The pendent droplet is assumed to be axisymmetric around vertical axis $z$. Let $P=(\boldsymbol{x}',\boldsymbol{z})$ be any point on the surface of the droplet with $\boldsymbol{x}'$ the axis obtained by rotation of $\boldsymbol{x}$ axis around $\boldsymbol{z}$ of angle $\phi$. The Cartesian coordinates of the point are related to its spherical coordinates $(\theta,\phi,r(\theta))$ can be expressed as:

$$\begin{aligned} x &= r(\theta)\sin\theta\cos\phi \\ y &= r(\theta)\sin\theta\sin\phi \\ z &= z_C - r(\theta)\cos\theta \end{aligned} \tag{5}$$

By introducing equation Eq. (4) to Eq. (5), we obtain:

$$\begin{aligned} r(\theta)\sin\theta\cos\phi &= x_0 + \alpha u_x \\ r(\theta)\sin\theta\sin\phi &= y_0 + \alpha u_y \\ z_C - r(\theta)\cos\theta &= z_0 + \alpha u_z \end{aligned} \tag{6}$$

The propagation distance $\alpha$ can be solved from Eq. (6):

$$\alpha = \frac{z_c - z_0 - r(\theta)\cos\theta}{u_z} \tag{7}$$

The rotation angle $\phi$ can be then obtained according to the Eq. (6):

$$\begin{aligned} \cos\phi &= \frac{x_0 + \alpha u_x}{r(\theta)\sin\theta} \\ \sin\phi &= \frac{y_0 + \alpha u_y}{r(\theta)\sin\theta} \end{aligned} \tag{8}$$

By using the fact $\cos^2\phi + \sin^2\phi = 1$ the angle $\theta$ is obtained by solving the following equation:

$$\begin{aligned} &(u_z x_0 + (z_c - z_0 - r(\theta)\cos\theta)u_x)^2 \\ &+(u_z x_0 + (z_c - z_0 - r(\theta)\cos\theta)u_y)^2 \\ &-u_z^2 r^2(\theta)\sin^2\theta = 0 \end{aligned} \tag{9}$$

Once the new interaction point is known, the local curvature matrix of the dioptric surface is calculated according to the surface function, and the wave front curvatures of reflected ray and the refracted ray are deduced from Eq. (1).

### 2.2.2. Calculation of the Total Scattered Intensity

The total scattered intensity in a given direction $(\theta,\phi)$ can be calculated according to the complex amplitude $E_{X,p}^n$ of all emergent rays arriving at that direction:

$$I^{no} = \sum_{n=0}^{N}\sum_{p=0}^{\infty}\sum_{X} I_{X,p}^n = \sum_{n=0}^{N}\sum_{p=0}^{\infty}\sum_{X}\left(E_{X,p}^n \cdot \left(E_{X,p}^n\right)^*\right) \tag{10}$$

where $n$ is the number of the rays, $p$ the order of the ray and $X$ the polarization state of the ray.

## 3. Simulation Results and Discussions

In this section, the SVCRM described in Section 2 will be used to analyze the scattered intensity distributions of pendent droplets by a vertically polarized plane wave. Here, the absorption in the particle is supposed negligible, so not taken into account in the simulation.

The pendant drop being circularly symmetric, its profile can be described by the distance of a point on the surface as function of the angle with the vertical direction $\theta$, i.e. $r(\theta)$. In our simulation, a 10th degree polynomial is used for $r(\theta)$, the coefficients of which are determined by the least-square fitting of the extracted curve from the contour of the particle image. The refractive index of the water droplet is $n_2 = 1.333$ and the wavelength of the incident plane wave is $\lambda = 632.8$ nm.

We will firstly compare in this section the results obtained by our simulation and the experiments, and then discuss the distribution of earch order of ray to understand the scattering mechanism.

### 3.1. Comparison of Numerical Results and Experimental Results

The schema of the experiment set-up is illustrated in Fig. 2. Two synchronized cameras are used to record simutaneously the particle image (Camera 1 in Fig. 2) and the scattering patterns in different positions by changing the position (Camera 2 in Fig. 2). A typical scattering pattern in forward direction is given in Fig. 3(a). We observe clearly a rainbow like arc bellow the spot (direct light) at about 35°, and a straight supernumery system appear and extend from the spot up with an angle of 30°, which does not exist for a spherical or elliptical particle. The shape of the first rainbows at 137° is similar to that of a spherical particle while the second order rainbow is completely deformed (Fig. 3(a)).

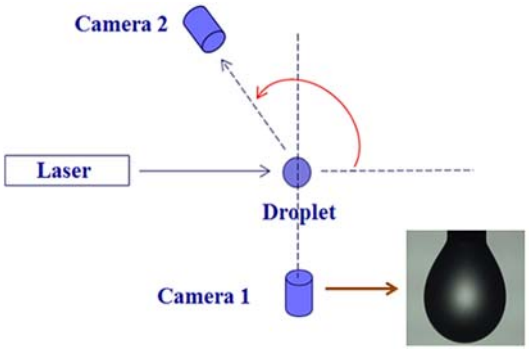



**Fig. 2.** Schematic diagram of experimental set-up.

The scattering patterns shown in Fig. 2 and Fig. 3 are simulated with SVCRM. The lateral diameter of

the droplet is 2.7 mm. The number of the incident rays is $2.4\times10^7$, which are used to express the properties of a plane wave. The simulated scattering patterns in forward and around the first and second rainbow angles are shown respectively in Fig. 3(b) and Fig. 4(b).

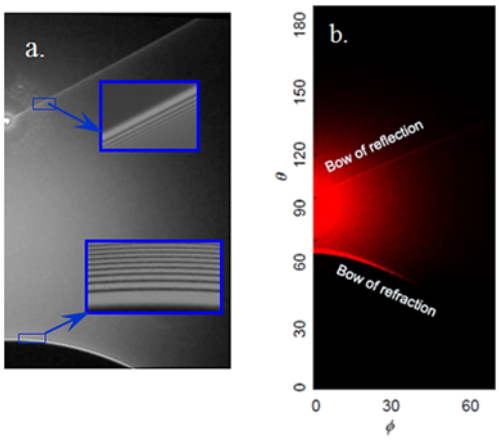



**Fig. 3.** Comparison of experimental simulated scattering patterns of a pendant droplet in forward direction.

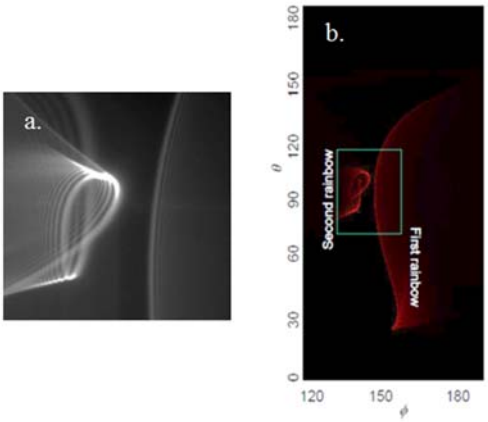



**Fig. 4.** Comparison of experimental simulated scattering patterns of a pendant droplet around rainbow angles.

## 3.2. Intensity Distributions of Different Orders

To reveal the scattering mechanism, the simulation has been done separately for different order rays. The profile of the drop is shown in Fig. 5. The lateral diameter of the particle is 1.304 mm. In the following simulation, the number of the incident rays is $4\times10^8$.

Fig. 6 shows the intensity distribution with $p=0$ (reflection rays only). We observe clearly a straight line appears and extend from the incident beam spot $(0,0)$ up with an angle of 25.5°, which is not the same with the 30° shown in the Fig. 3(b). That can be interpreted as a difference in the particle shape. This particle is more elongated than that in Fig. 3.

For the order $p=1$, the rays experience two refractions through the droplet. Fig. 7 displays the intensity distribution. We identify clearly a rainbow like arc extend from the point $(0^\circ,-20.5^\circ)$, which is also different from the 35° shown in Fig. 3(b).

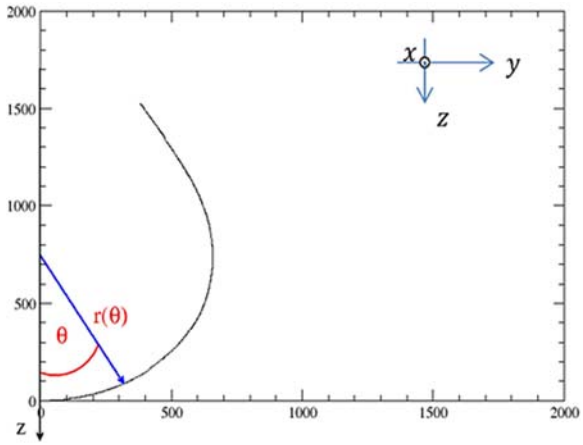



**Fig. 5.** Half of a pendent droplet profile in Cartesian coordinate system the lateral diameter of the droplet is 1.304 mm.

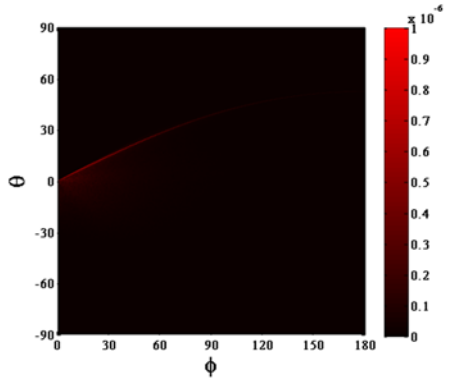



**Fig. 6.** Intensity distribution with $p=0$.

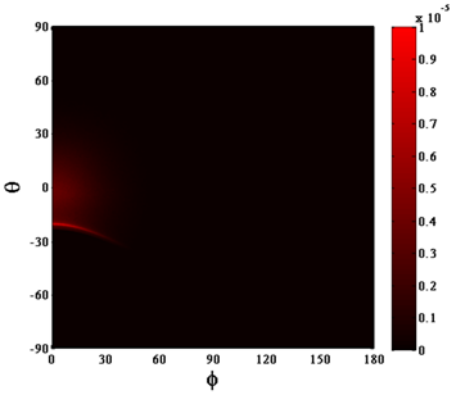



**Fig. 7.** Intensity distribution with $p=1$

The first order rainbow is generated in a pendant droplet as in a spherical particle by the rays which

have undergone one internal reflection ( $p = 2$ ). We can observe from Fig. 8 that the arc is similar to the rainbow of a spherical droplet near the horizontal plane $\theta = 0^{\circ}$ but deformed when relatively large angle $\theta$ .

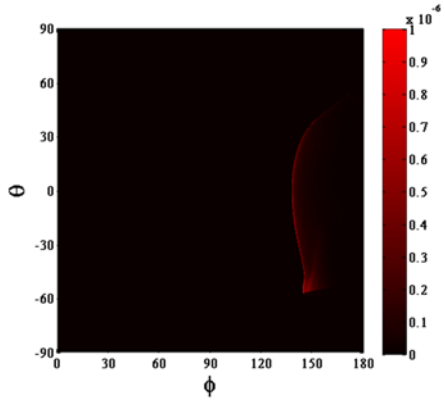



**Fig. 8.** Intensity distribution with $p = 2$ .

When $p = 3$ , the rays experience two internal reflections (Fig. 9). The second order rainbow is no longer a circular bow as in the spherical particle but completely twisted to a form like earring.

For the order $p = 4$ , the intensity distribution is given in Fig. 10. The maximum intensity is located at 40.71° with $\theta = 0^{\circ}$ . It is worthy to note that the intensity is much weaker than $p = 3$ due to one more internal reflection.

The total intensity is shown in Fig. 11, we observe the intensity in forward direction ( $p : 0 \sim 1$ ) much stronger than the contributions of others orders. The first and the second rainbows ( $p : 2 \sim 3$ ) are also clearly visible, with the second rainbow stronger the first one, different from the intensity ratio of these two orders in a spherical droplet. The intensity of the order $p = 4$ is so weak compared to the other orders that it is invisible in this figure.

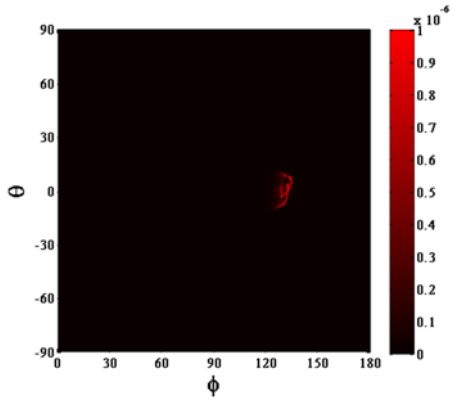



**Fig. 9.** Intensity with $p = 3$ .

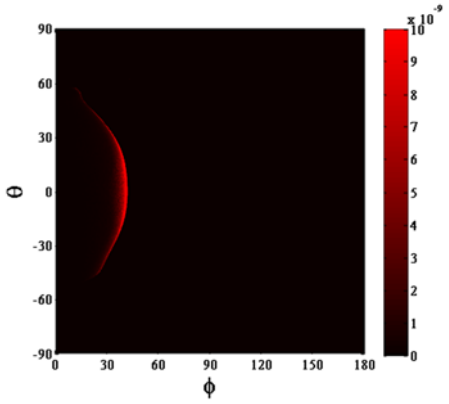



**Fig. 10.** Intensity with $p = 4$ .

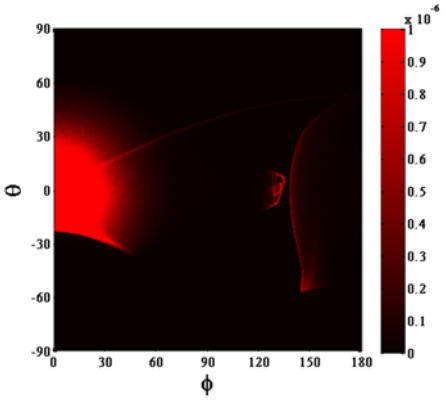



**Fig. 11.** Intensity distribution with $p : 0 \sim 4$ .

For more detail information, Fig. 12 shows the scattering patterns around around rainbow angles.

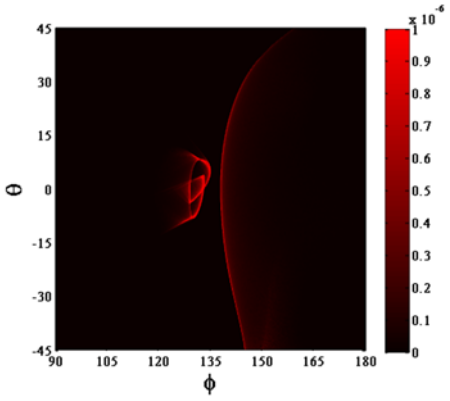



**Fig. 12.** Intensity distribution with $p : 2 \sim 3$ .

## 4. Conclusions

The Statistic Vectorial Complex Ray Model is explored and applied to the simulation of pendant droplets. The simulated scattering patterns agree well with the skeletons of the images obtained experimentally and scattering mechanisms of different orders are identified. We are working on the

interference between different orders in order to exploit the Airy like structure in forward direction and near rainbow angles.

## Acknowledgements

The authors acknowledge the support from the China Scholarship Council for the stay of Ruiping YANG at CORIA. This work has been also partially supported by the French National Research Agency, France under the grant ANR-13-BS090008-01 (AMO-COPS) and CRIANN (Centre Régional Informatique et d'Applications Numériques de Normandie).

## References

[1]. H. C. van de Hulst, Light scattering by small particles, *Courier Corporation*, 1957.

[2]. F. Xu, K. F. Ren, G. Gouesbet, X. Cai, G. Gréhan, Theoretical prediction of radiation pressure force exerted on a spheroid by an arbitrarily shaped beam, *Phys Rev E*, Vol. 75, Issue 2, 2007, 026613.

[3]. K. F. Ren, F. Onofri, C. Rozé, T. Girasole, Vectorial complex ray model and application to two-dimensional scattering of plane wave by a spheroidal particle, *Optics Letters*, Vol. 36, Issue 3, 2011, pp. 370-372.

[4]. K. F. Ren, C. Rozé, Vectorial Complex Ray Model for light scattering of non-spherical particles, in Advances in Optics: Reviews, Book Series, Vol. 1, Chapter 7, *IFSA Publishing*, 2018.

[5]. M. Yang, Y. Wu, X. Sheng, K. F. Ren, Comparison of scattering diagrams of large non-spherical particles calculated by VCRM and MLFMA, *Journal of Quantitative Spectroscopy and Radiative Transfer*, Vol. 162, 2015, pp. 143-153.

[6]. F. Onofri, K. F. Ren, M. Sentis, Q. Gaubert, C. Pelcé, Experimental validation of the vectorial complex ray model on the inter-caustics scattering of oblate droplets, *Optics Express*, Vol. 23, Issue 12, 2015, pp. 15768-15773.

[7]. R. P. Yang, C. Rozé, S. Idlahcen, K. F. Ren, Simulation of Light Scattering from Large Non-spherical Particles by Statistic Vectorial Complex Ray Model, in *Proceedings of the 1st International Conference on Optics, Photonics an Laser (OPAL'2018)*, Barcelona, Spain, 9-11 May 2018, pp. 118-119.

Published by International Frequency Sensor Association (IFSA) Publishing, S. L., 2018 (http://www.sensorsportal.com).

